IEEE Access
Multidisciplinary | Rapid Review | Open Access Journal

Received October 6, 2021, accepted October 26, 2021, date of publication November 15, 2021, date of current version November 19, 2021.

Digital Object Identifier 10.1109/ACCESS.2021.3128190

Multi-Band Multi-Functional Metasurface-Based Reflective Polarization Converter for Linear and Circular Polarizations

RAHUL DUTTA[1], JEET GHOSH[2], ZHENGBAO YANG[3], (Member, IEEE), AND XINGQI ZHANG[4], (Member, IEEE)

[1]School of Electronics Engineering and Computer Science, Queen Mary University of London, London E1 4NS, U.K.
[2]Department of Electronics and Communication Engineering, Chaitanya Bharathi Institute of Technology, Hyderabad 500075, India
[3]Department of Mechanical Engineering, City University of Hong Kong, Hong Kong
[4]School of Electrical and Electronic Engineering, University College Dublin, Dublin 4, D04 V1W8 Ireland

Corresponding author: Xingqi Zhang (xingqi.zhang@ucd.ie)

ABSTRACT In this paper, we present a simple metasurface based multiband reflective polarization converter for both linear and circular polarizations. We show that, on one hand, the proposed structure can convert the polarization of linearly polarized waves to the orthogonal direction at four frequency bands — 4.3 GHz, 7.2 GHz, 12.3 GHz, and 15.15 GHz. On the other hand, this metasurface can achieve linear to circular or circular to linear polarization conversion at 4 GHz, 4.75–5.95 GHz, 8.35–8.8 GHz and 14.35–14.6 GHz frequency bands. Such multiband operation originates from multiple resonances occurring in the structure based on meandered square ring and diagonal split strip resonator. Moreover, the polarization transforming capability is stable for oblique incident angle up to 15^o, for both transverse electric (TE) and transverse-magnetic (TM) polarizations. Furthermore, the proposed structure acts as a meta-reflector that maintains the handedness of the circular polarization upon reflection. Finally, a prototype of the proposed meta-structure is fabricated and measured for both normal and oblique incidence of electromagnetic waves. All the results present excellent resonant stability with respect to the different polarization and incident angles. In addition, we have also performed the tolerance analysis of different material parameters to understand the robustness of the structure. Due to the ability of the structure to perform three functionalities through a single layout, the proposed design can pave its way in different microwave applications such as satellite, radar, and 5G communications.

INDEX TERMS Polarization converter, multi-functional, multi-band, linear polarization, circular polarization.

I. INTRODUCTION

Metasurfaces, also known as two-dimensional metamaterials, are sub-wavelength artificial structures that are used to modulate the propagation of electromagnetic (EM) waves. Due to its unconventional ability to achieve unique EM properties, metasurfaces have received huge recognition in the past decades. Such manipulation of EM waves has led to diverse applications such as absorber [1], [2], cloaking [3], [4], lensing [5], [6], and polarization converter [7], [8], which are greatly influencing our day-to-day lives. Particularly, the metasurface based polarization converter are used in several application such as controlling the polarization of radiating wave [9], [10], and radar cross section (RCS) reduction [11], [12], etc. In [9], a metasurface is used over the linear polarized slot antenna to convert the polarization of radiated wave. Similarly, a mirror polarization conversion metasurface is used in [10] for manipulating the polarization of the radiated wave. Beside these, different arrangement of the polarization converting metasurface can also be used to reduce the RCS of any object [11], [12].

Polarization converters are devices that can change the polarization state of an EM wave. Before the advent of metasurfaces, researchers proposed devices made of natural materials using optical activity crystals or Faraday effects. However, such approaches are bulky in nature and required

The associate editor coordinating the review of this manuscript and approving it for publication was Debabrata Karmokar.

a long propagation distance to obtain the phase accumulation, thus limiting their practical applications [13]. These limitations were easily overcome by the introduction of metasurface-based polarization converters.

With this notion, several researchers have developed metasurfaces that can alternate the polarization of the incoming wave either in transmission or in reflection mode. However, in order to achieve higher transmission efficiency in the transmission mode, the metasurface needs to be made thin to reduce losses. Thus, reflection mode of operation is usually preferred, as higher efficiency can be accomplished due to the total reflection of the incident waves. Again, the reflective polarization converters are fabricated over the metal-backed dielectric layers. The metal backing not only restricts the transmission of the electromagnetic waves but also has a significant influence on the resonance frequency.

Through the use of the metasurface-based polarization converters, various manipulation of EM waves such as linear orthogonal polarization conversion (LP-LP) [14], [15], linear polarization to circular polarization (LP-CP) [16], [17], and circular to circular polarization (CP-CP) [18], [19], has been achieved. However, the above mentioned polarization converters are based on singular functionality and due to the advancement in technologies, there is a great demand for structures serving more than one function. With this motivation, few researches on multiple conversion, such as LP to LP, LP to CP, of EM waves with the help of a single metasurface have been reported. In [20], a reflective polarization converter, which works for LP-LP and CP-CP conversions, is proposed. In another work [21], a dual band reflective polarization converter has been reported, where LP-LP is achieved in one band and LP-CP is achieved in another band. Nevertheless, none of the structures [20], [21] accomplishes conversion of LP wave to both left-handed (LHCP) and right-handed circular polarizations (RHCP). In our article, we theoretically and experimentally determine a compact, ultrathin reflective polarization converter that can achieve different polarization conversions at multiple frequency bands. We present that different operations like LP-LP, LP-LHCP and LP-RHCP can be integrated simultaneously into a single layer metasurface. Linear polarization has been obtained at four resonances, whereas, circular polarizations (LHCP and RHCP) are achieved at another four frequencies. Thus, the proposed reflective polarization converter can be considered as a eight-band multi-functional polarization converter. Further, the design is also tested for angular stability. Finally, the structure is fabricated and verified in experiments to confirm its practicability.

The rest of this article is organized as follows. Section II describes the design methodology of the metasurface to control the polarization of the electromagnetic waves. Initially, we have discussed the basic physics behind the polarization conversion techniques with the help of a 4-port network and eigenvector analysis. In the subsequent part of this section, the reflection property of the metasurface has been studied. Here, we have explained the step-by-step procedure for designing the reported metasurface. The cause of polarization conversion phenomena is investigated with the help of surface current distributions. Section III presents measurement responses of the proposed polarization converter in comparison with the simulated responses. Finally, the conclusion of this article followed by the state-of-the-art performance comparisons have been made in Section IV.

II. DESIGN METHODOLOGY

The schematic view of the proposed metasurface as reflective polarization converter is shown in Figure 1(a). The metasurface consists of two dimensional array of metallic pattern fabricated over a metal backed dielectric substrate. Each element of the metallic array comprises a diagonal strip and a meandering square ring as shown in Figure 1(b). The square ring has a slit positioned at the corner aligned with the gap in the diagonal strip. The structure is printed on the top surface of a metal-backed dielectric FR4 substrate (permittivity, $\epsilon_r = 4.4$; loss tangent, $\delta = 0.02$) with 3.2 mm thickness. The optimized geometrical dimensions of the proposed structure are summarized in Table 1.

TABLE 1. Optimized geometrical dimension values (in mm).

p	a_1	a_2	a_3	a_4	w_1	w_2	g
11	3	2.5	8	1	0.5	0.4	0.5

A. THEORETICAL ANALYSIS

To understand the polarization conversion mechanism, we need to focus on the physical insight of the polarization conversion. Initially, consider a square shaped unit cell with a rectangular metallic strip. It should be noted that, for simplicity, we consider negligible metallization thickness. The structure is fabricated over a dielectric substrate and is symmetric over *X*- and *Y*-axis. The conceptual diagram is shown in Figure 2(a). It is observed that the unit cell exhibits two symmetries in both horizontal (H) and vertical (V) planes. If the electric field of normal incidence electromagnetic wave is polarized along the vertical axis or Y-axis, the reflecting/transmitting wave does not generate any horizontal component or *X*-axis component. A similar phenomenon is observed for the electromagnetic wave incidence along *X*-axis. Thus, both polarizations are decoupled and can be described independently. In this regard, the equivalent circuit of the unit cell of Figure 2(a) needs to be expressed separately for horizontal and vertical polarization as shown in Figure 2(b). From the above discussion, we can state that the unit cell of Figure 2(a) is unsuitable for converting the polarization of the electromagnetic wave.

In the next step, we analyzed a unit cell which is asymmetric along the X- and Y-axis as shown in Figure 2(c). In this case, the cell will generate both horizontal and vertical component of the electric field. The unit cell shown

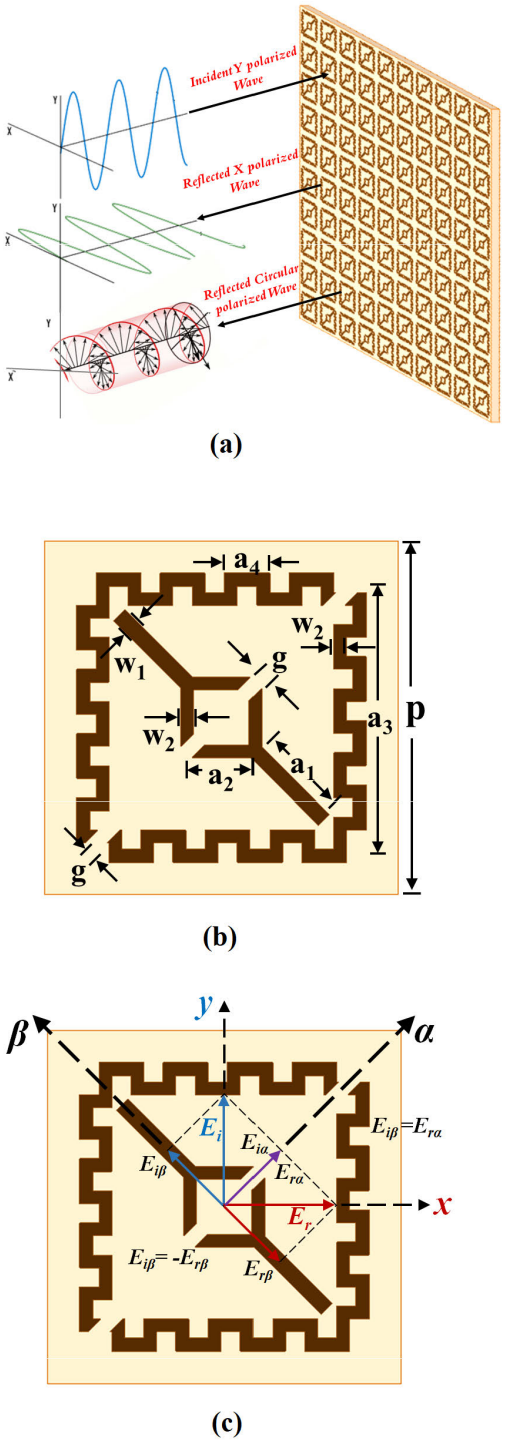

FIGURE 1. (a) An artistic rendering of the proposed reflective polarization converter structure (b) Schematic view of the unit cell of proposed reflective polarization converter (c) Decomposition of an incident y-polarized wave in its two components and its conversion to x-polarized wave.

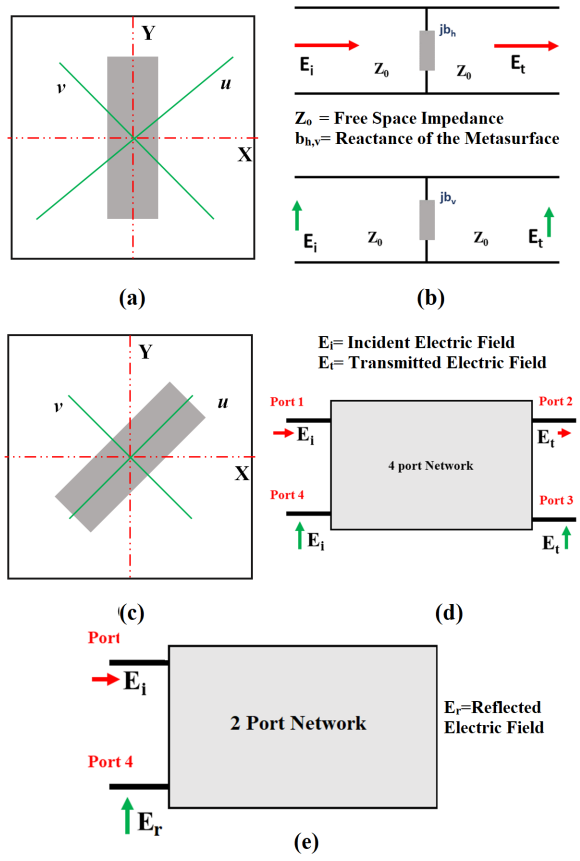

FIGURE 2. Schematic model of the unit cell (a) Symmetry along X- and Y-axis (b) two-port network model of symmetric unit cell (c) Asymmetric unit cell along X- and Y-axis (d) four-port network model of the asymmetric unit cell (e) Network model of the unit cell with metal backed, i.e, no transmission.

in Figure 2(c) can be modelled as a four port network as shown in Figure 2(d). Each port of the network is associated with a specific polarization, such as horizontal and vertical polarization. In a reflective type polarization converter, there will be negligible transmission of electromagnetic wave from input port to the output port. Thus, all the transmission coefficient of the network, such as S_{ij}, $i = 1, 4$ and $j = 2, 3$, are equal to zero. The S matrix of the metal backed reflective polarization converter can be expressed as

$$S = \begin{bmatrix} S_{11} & 0 & 0 & S_{14} \\ 0 & 1 & 0 & 0 \\ 0 & 0 & 1 & 0 \\ S_{14} & 0 & 0 & S_{11} \end{bmatrix} \tag{1}$$

In the Figure 2(e), we simplified the four port model for reflective polarization converter. The simplified matrix can be expressed as

$$S = \begin{bmatrix} S_{11} & S_{14} \\ S_{14} & S_{11} \end{bmatrix} = R \tag{2}$$

In this equation, S_{11} indicates the co-polarized reflection coefficient (R_{xx}) whereas S_{14} denotes the cross-polarized reflection coefficient (R_{yx}). By controlling the magnitude of this coefficient, we can attain the desired polarization conversion from a metasurface.

In accordance with the above explanation, the process of achieving a metasurface based polarization conversion can also be considered as a linear time invariant system (LTI). Here, the input vector is the incident electromagnetic wave, which is transformed to the output vector, i.e., polarization converted reflected wave. Thus, the incident electric field $[E_{ix}\ E_{iy}]^T$ and the reflected electric field $[E_{rx}\ E_{ry}]^T$ can be related as

$$\begin{bmatrix} E_{rx} \\ E_{ry} \end{bmatrix} = \begin{bmatrix} R_{xx} & R_{xy} \\ R_{yx} & R_{yy} \end{bmatrix} \begin{bmatrix} E_{ix} \\ E_{iy} \end{bmatrix} \tag{3}$$

Here, R_{ij} is the reflection coefficient in which the incident linear polarization is denoted by 'j' while the reflected polarization is denoted by 'i'. Thus, for a ideal polarization converter, the co-polarization reflection coefficient $R_{xx} = R_{yy} = 0$ and cross-polarization reflection coefficient $R_{xy} = R_{yx} = 1$. Thus the reflection matrix for a polarization converter can be expressed as

$$R = \begin{bmatrix} 0 & 1 \\ 1 & 0 \end{bmatrix} \tag{4}$$

In the following step, we need to find out the eigenvalues and eigenvectors for the polarization converting metasurface. The obtained eigenvectors are $\alpha = [1\ 1]^T$ and $\beta = [-1\ 1]^T$ with eigenvalues $e^{i0} = 1$ and $e^{i\pi} = -1$ respectively. Physically, this implies that when the electric field is oriented along the direction of α and β eigenvector, which is tilted by $\pm 45^0$ to the y-axis, the reflected wave does not face any polarization rotation. As there is no polarization rotation along the α and β axes, we can state that

$$\begin{aligned} R_{\alpha\alpha} &= R_{\beta\beta} \approx 1 \\ R_{\alpha\beta} &= R_{\beta\alpha} \approx 0 \end{aligned} \tag{5}$$

Therefore, a normally incident y-polarized wave with electric field $E_y = \hat{y}E_i e^{ikz}$ can be written by the sum of two mutually orthogonal components in the direction of $\hat{\alpha}$ and $\hat{\beta}$ as

$$\mathbf{E_i} = (\hat{\alpha}E_{i\alpha} + \hat{\beta}E_{i\beta})e^{ikz} \tag{6}$$

In this equation, $E_{i\alpha} = E_{i\beta} = 0.707E_i$. As α and β components of the electric field are the eigenvectors, thus they are reflected with the same magnitude, $E_{r\alpha} = E_{r\beta} = 0.707E_r$, with 0^o and 180^0 phase respectively. Thus, the reflected field is expressed as

$$\mathbf{E_r} = (\hat{\alpha}E_{r\alpha} - \hat{\beta}E_{r\beta})e^{ikz} = \hat{\mathbf{x}}E_r \tag{7}$$

From Eq. (7), it can be stated that the y-polarized incident EM wave is reflected along the x-axis. Thus the polarization of the wave is rotated by 90°. This phenomenon is illustrated in Figure 1(c) where the reflected electric field E_r, obtained from the vector sum of $E_{r\alpha}$ and $E_{r\beta}$, is along the x-axis. As discussed earlier, for the cross-polarization conversion, the phase difference between $\hat{\alpha}$ and $\hat{\beta}$ should be an odd multiple of 180^o, i.e. $\Delta_{\alpha\beta} = ang(R_{\alpha\alpha}) - ang(R_{\beta\beta}) = n\pi$ (n = odd integer).

From Eq. (6) and Eq. (7), it can be said that the electric field of reflected wave can be expressed as

$$\mathbf{E_r} = (\hat{\alpha}R_{\alpha\alpha}E_{i\alpha}e^{i\phi_{\alpha\alpha}} - \hat{\beta}R_{\beta\beta}E_{i\beta}e^{i\phi_{\beta\beta}})e^{ikz} \tag{8}$$

As the polarization reflected field is perpendicular to the incident wave, $E_i \cdot E_r = 0$. So, at $z = 0$,

$$E_{i\alpha}e^{i\phi_{\alpha\alpha}}(1 + e^{i\Delta\phi}) = 0 \tag{9}$$

It can only be possible if $\Delta\phi = n\pi$ for $n = \pm 1, \pm 3, \cdots$.

B. RESULTS AND DISCUSSION

To comprehend the polarization conversion performance of the proposed structure, the numerical simulation of our design is executed using Ansys HFSS. In the simulations, we have utilized Floquet ports to excite the structure accompanied by master-slave boundary conditions for realizing an infinite array condition. Given the fact that the designed reflective polarization converter is anisotropic in nature, any incident LP wave on such a structure gets reflected with both co- and cross-polarized components. This can be seen from Figure 3 (a) that the co-polarized reflection R_{xx} is less than -10 dB whereas the cross-polarized reflection R_{yx} is greater than -1 dB at three frequencies, i.e. 4.3, 7.2, and 12.3 GHz along with around -2.5 dB at 15.15 GHz. Additionally, the relative phase difference between R_{xx} and R_{yx} at these four resonating frequencies is also monitored. The relative phase difference is defined as,

$$\Delta\phi = arg(R_{yx}) - arg(R_{xx}) \tag{10}$$

The essence of polarization is identified from Eq. (10) in the sense that if, $\Delta\phi = 0, \pm\pi$, then it is characterized as linear polarized [8]. From Figure3(b), it can be observed that at 4.3, 7.2, 12.3 and 15.15 GHz, the phase differences are around 180°, $-180°$, 0° and 180° respectively. For analyzing the reflective phase response more clearly, we have also plotted the unwrapped relative phase ($\Delta\phi$) and depicted it in Figure 3(c). It is observed that, in the orthogonal polarization conversion band, the relative unwrapped phase is equal to $\pm n\pi$, whereas n is equal to any integer. To analyze the performance of the polarization converter structure, $R_{\alpha\alpha}$ and $R_{\alpha\beta}$ is also computed and plotted in Figure 4(a). It is observed that, as expected from the theoretical analysis and Eq (5), $R_{\alpha\alpha} = 1$ and $R_{\alpha\beta} = 0$ at the desired frequency region. Furthermore, we have also monitored the phase response with respect to α and β co-ordinates and observed that the phase response at our desired frequency band is always equal to $n\pi$ as mentioned in Figure 4(b).

In addition, the polarization conversion ratio (PCR) of the proposed structure is also calculated and shown in Figure 5. The PCR for linear polarization is defined as,

$$PCR = \frac{R_{yx}^2}{R_{yx}^2 + R_{xx}^2} \tag{11}$$

From Figure 5, it can be seen that the PCR at the four resonating frequencies are 98.08%, 99.90%, 98.55%

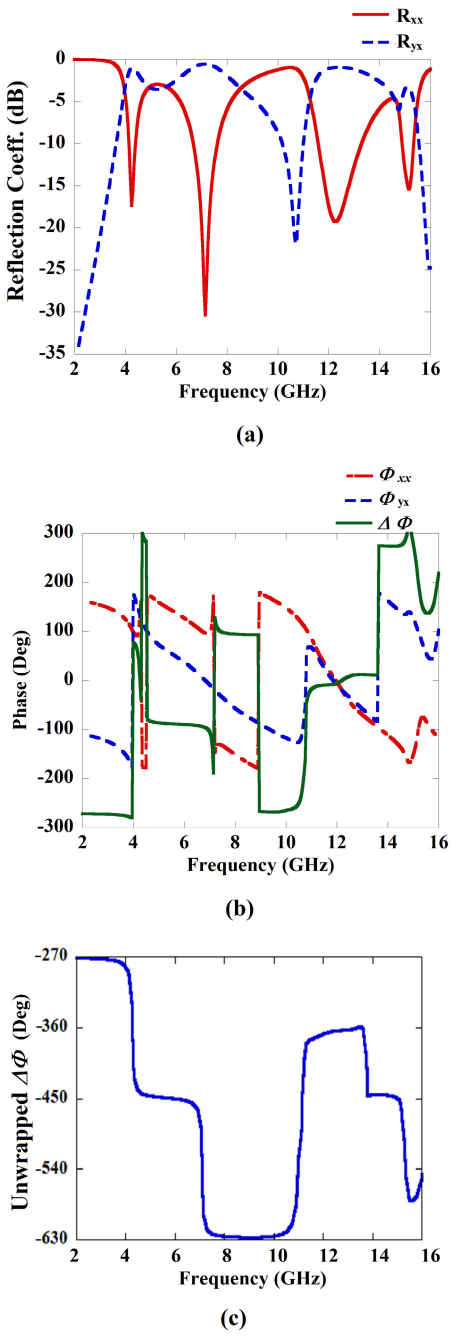

FIGURE 3. Reflection performance of the proposed octa-band reflective polarization converter design (a) Magnitude of the reflection coefficient (b) Phase of the reflection coefficient (c) Unwrapped relative phase of the reflected electromagnetic wave.

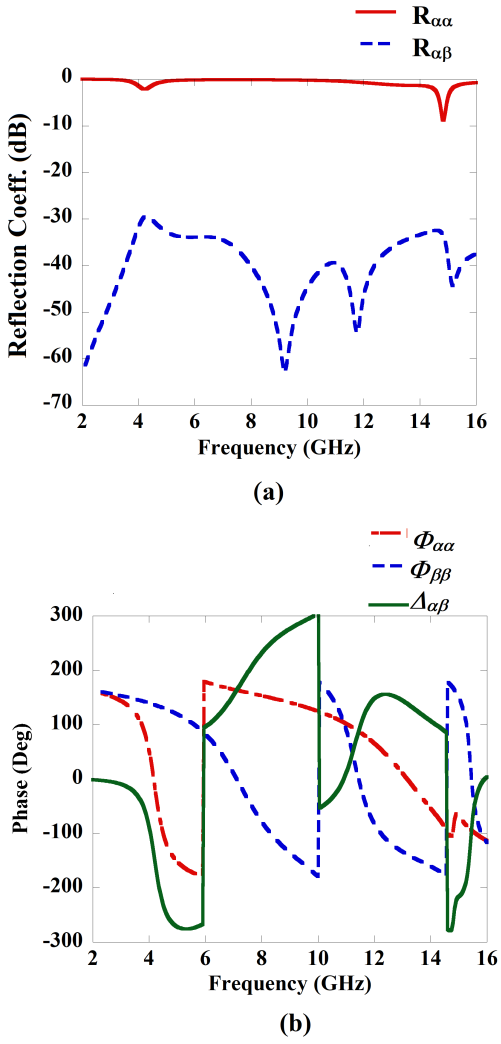

FIGURE 4. Reflection performance of the proposed octa-band reflective polarization converter design along α- and β-axis (a) Magnitude of the reflection coefficient along α- and β-axis (b) Phase of the reflection coefficient along α- and β-axis.

and 95.16%. Thus, it can be inferred that any incident EM wave on the proposed structure gets converted to its orthogonal counterpart at these four resonating frequencies. To get a clear understanding regarding the design procedure of the proposed reflective polarization conversion structure, here we dissociate the final proposed geometry into several separate components. Initially, we should mention that, for converting the polarization of incident electromagnetic wave, the structure of the unit cell should be asymmetric along the horizontal and vertical axis and symmetric along the diagonal axis or the U- and V-axis as shown in Figure 2(b). By considering the above mentioned fact, we start our design with a diagonal strip dipole structure as shown in Figure 5(a) along with the *PCR* of the structure. It is observed that the diagonal strip dipole provides *PCR* of 70% at 15.6 GHz frequency. It should be mentioned that, for converting the polarization of the incident wave, the *PCR* should be around 100%. So, to enhance the *PCR* of the structure, we add an inverted arrowhead with the cross dipole structure. This structure is termed as Reso.I. in the following text. The *PCR* of the Reso.I is shown in Figure 5(a). It is observed from the figure that the Reso.I structure provides *PCR* more than 95% at 15.15 GHz frequency. To understand the aforementioned phenomenon, we also monitor the electric field distribution along the surface of the unit cell structure, such as diagonal

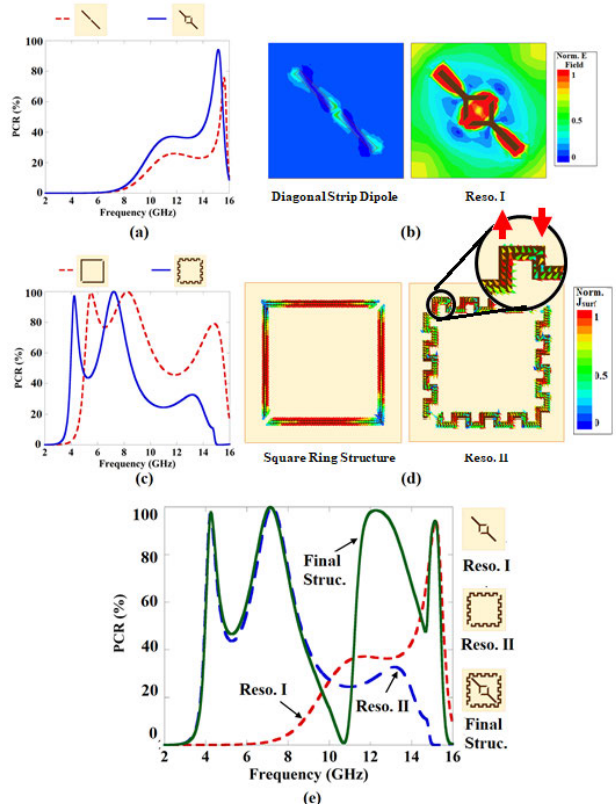

FIGURE 5. Step-by-step analysis of the metasurface (a) Analysis of PCR for Reso. I structure (b) E-Field distribution of the diagonal strip structure and Reso. I (C) Analysis of PCR for Reso. II structure (d) Surface current distribution of the square ring structure and Reso II. and (e) PCR analysis of the final metasurface.

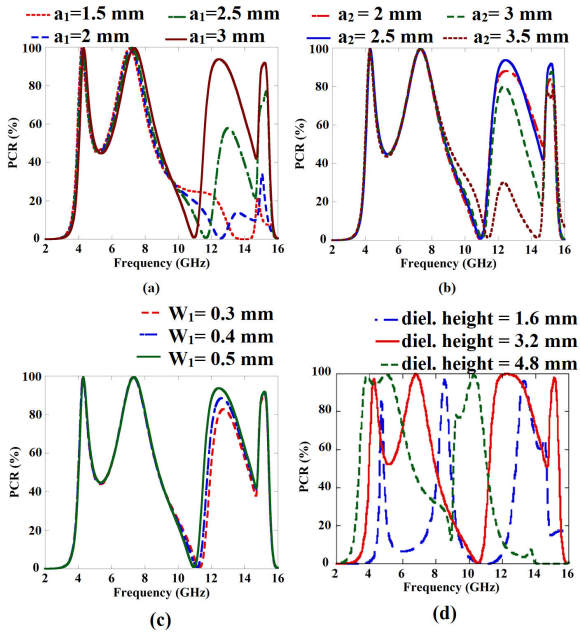

FIGURE 6. Simulated polarization conversion ratio for different values of (a) a_1 and (b) a_2 (c) w_1 and (d) dielectric height.

strip structure and Reso. I structure, as shown in Figure 5(b). It is observed that, by adding an inverted arrow over the diagonal strip, a strong electric field accumulated along the diagonal of the unit cell. Due to the diagonal distribution of the E-Field, the *PCR* of the structure gets enhanced to more than 95%. To achieve multi-band resonance structure, several resonator structure should be cascaded to each other. For this purpose, we design a diagonal slot square ring structure. The diagonal slot square ring structure is shown in Figure 5(c). It is observed that, the PCR is more than 95% at frequency 5.8 GHz. Since, our main goal is to design a reflective polarization converter for C, X and Ku bands, so, in order to achieve the polarization conversion at the lower part of the C band, one need to increase the reactance part of the resonator. Particularly, here we enhance the inductance of the structure by increasing the electrical length of the resonator structure. In this regard, we meander the square ring structure and the modified resonator is termed as Reso.II. It is also observed in Figure 5(c) that Reso.II provides *PCR* is more than 95% in lower part of the C band which is more important for satellite communication. It is worth mentioning that, the *PCR* of the Reso. II at the resonating frequency region is comparable with the PCR of the square ring structure. For understanding this electromagnetic behaviour, we plotted the surface current distribution along the metallic layer of the square ring and Reso. II structure, as shown in Figure 5(d). It is observed that, due to the meandering of the structure, the orthogonal anti-parallel current components are created (encircled by black in the figure) each of the adjacent arms. Because of the anti parallel distribution, the orthogonal current components are cancelled out by each other. As a result of this, the *PCR* of the meander square ring structure is not deteriorated at the resonating frequency region.

To achieve the desired multiband polarization converter, the two resonator structures, i.e, Reso.I and Reso.II, are cascaded. From the Figure 5(a) and 5(c), we can state that Reso.I is responsible for achieving polarization conversion band at the higher frequency region whereas control over the lower frequency region is achieved with Reso.II. It is observed that, due to the cascading of Reso.I and Reso.II structure, four orthogonal polarization conversion band is achieved. The mid frequency band around 12.3 GHz is achieved due to the coupling between Reso.I and Reso.II.

For the purposes of obtaining the desired functionality of the proposed structure, we analyzed the polarization conversion ratio by optimizing the values of different parameters such as, a_1, a_2, and the strip width w_2 and exhibited the results in Figure 6. From this parametric study, it is observed that the parameters a_1 and a_2 have a huge impact on the polarization conversion ratio at the 12-14 GHz frequency region. It is also seen from Figure 6(a) that, with increase in a_1, the PCR in the higher frequencies improves significantly. However, a_1 is not increased above 3 mm as it would lead to short-circuit between Reso.I and Reso.II. Besides this, the strip width w_2 also provides a significant impact on the *PCR*. Moreover, we also analyze the effect of substrate height over the *PCR* of the metasurface and plotted in Figure 6(d). It is observed that,

as the height increases, the metasurface provides better *PCR*. However, at 4.8 mm height, the proposed structure provides orthogonal polarization conversion at only two frequency bands and also does not cover the entire operating frequency region. Additionally, the substrate height of 4.8 mm also makes the structure bulky and may not be suitable for several compact applications. For this aforementioned reasons, we designed the metasurface over a substrate of 3.2 mm, which provides multiband features in the desired frequency regions.

Alongside the orthogonal polarization conversion of the linear polarized wave, we also need to investigate the response of the proposed reflective polarization converter under the incidence of circularly polarized EM wave. In the previous discussion of this section, we already obtained the magnitude and phase of the reflection coefficient of the metasurface on a rectangular basis. We can easily transform these responses into circular basis using [22]

$$R_{CP} = \begin{bmatrix} R_{RR} & R_{RL} \\ R_{LR} & R_{LL} \end{bmatrix} = \frac{1}{2}\begin{bmatrix} R_{xx}-R_{yy}-i(R_{xy}+R_{yx}) & R_{xx}+R_{yy}+i(R_{xy}-R_{yx}) \\ R_{xx}+R_{yy}-i(R_{xy}+R_{yx}) & R_{xx}-R_{yy}+i(R_{xy}+R_{yx}) \end{bmatrix} \tag{12}$$

In this equation, the subscript 'R' indicate right-hand circular polarized (RHCP) wave whereas subscript 'L' indicates left hand circularly polarized (LHCP) wave. It should be mentioned that, when a RHCP polarized wave incidents over a metallic reflector or mirror, it gets reflected as LHCP wave and vice versa. From the Eq. (12), it is observed that when $R_{xx} = R_{yy} = 0$ and $R_{xy} = R_{yx} = 1$, then $R_{RR} = R_{LL} = 1$. Thus, from the above equation, we can state that when a CP wave incidents over the metasurface, the reflected wave have the same essence of polarization at the aforementioned frequency band (4.3, 7.2, 12.3, and 15.15 GHz). The polarization maintaining capability is captured by defining polarization maintaining ratio (PMR) for circular polarization as

$$PMR = \frac{|R_{RR}|^2}{|R_{LR}|^2 + |R_{RR}^2|} \tag{13}$$

From the above analysis, it can be stated that PMR for the circular polarization is the same as *PCR* in the orthogonal polarization conversion band. Thus, in these frequency bands $R_{RR} = R_{LL} = R_{xy} = R_{yx} = 1$ and $R_{LR} = R_{RL} = R_{xx} = R_{yy} = 0$. Thus the proposed structure can be treated as a meta-reflector that preserves handedness of the circular polarization upon reflection at 4.3, 7.2, 12.3, and 15.15 GHz frequency regions.

On the other hand, to analyse the linear-to-circular polarization conversion properties of the metasurface, it is necessary to be mindful of two important facts that, for circular polarization,

(1) the amplitudes of the two mutually orthogonal EM waves must be identical,

(2) their relative phase difference should be odd multiples of 90°, i.e. $\Delta\phi = n\pi/2$, where n is an odd integer.

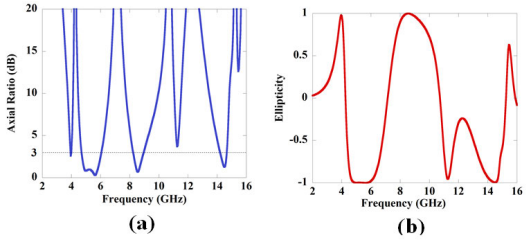

FIGURE 7. (a) Axial ratio and (b) Ellipticity of the proposed reflective polarization converter structure.

As can be perceived from Figure 3(a), the difference in magnitudes of both co- and cross-polarized reflected wave are almost negligible at the frequency regions: 4, 4.75–5.95, 8.35–8.8 and 14.35–14.6 GHz, indicating that the two mutually orthogonal reflected waves have nearly equal amplitudes at those frequency bands. Further, the phase difference plot provided in Figure 3(b), shows that $\Delta\phi$ at these four frequency regions is 90°, −90°, 90° and 270°, respectively. From the unwrapped phase plot in Figure 3(c), it is observed that the $\Delta\Phi$ at the mentioned frequency is $n.\frac{\pi}{2}$, where n = odd integer.

In order to have a clear estimation on the achievement on polarization conversion and the handedness of the reflected circular polarization, we calculate the axial ratio (AR) and the ellipticity. The axial ratio is determined by the formula [23] defined as follows:

$$AR = \frac{1}{2}\left\{\frac{|R_{xx}|^2 + |R_{yx}|^2 + \sqrt{a}}{|R_{xx}|^2 + |R_{yx}|^2 + \sqrt{a}}\right\}^{\frac{1}{2}} \tag{14}$$

where,

$$a = |R_{xx}|^4 + |R_{yx}|^4 + 2|R_{xx}|^2|R_{yx}|^2 cos(2\Delta\phi) \tag{15}$$

The AR signifies circular polarization if it is less than or equal to 3 dB, i.e. $AR \leq 3$ dB. The calculated AR obtained from Eq. (14) is plotted in Figure 7(a). It can be seen from the figure that the convention for the establishment of circular polarization is clearly met at the frequency regions: 4 GHz, 4.75–5.95 GHz, 8.35–8.8 GHz, and 14.35–14.6 GHz. Thus, it can be concluded that the proposed reflective polarization converter structure is capable of performing linear-to-circular polarization conversion at these four frequency bands.

On a related note, the definition of normalized ellipticity (e) for the determination of the handedness of the circular polarization [22] is given by,

$$e = \frac{2|R_{xx}||R_{yx}|sin(\Delta\phi)}{|R_{xx}|^2 + |R_{yx}|^2} \tag{16}$$

For the sake of simplicity, it can be stated from Equation (16) that for left-handed circular polarization (LHCP), the normalized ellipticity is −1, whereas the latter is +1 for right-handed circular polarization (RHCP). It should be mentioned that, the above analysis is performed for the normal incidence of EM wave. From Figure 7(b), it can be

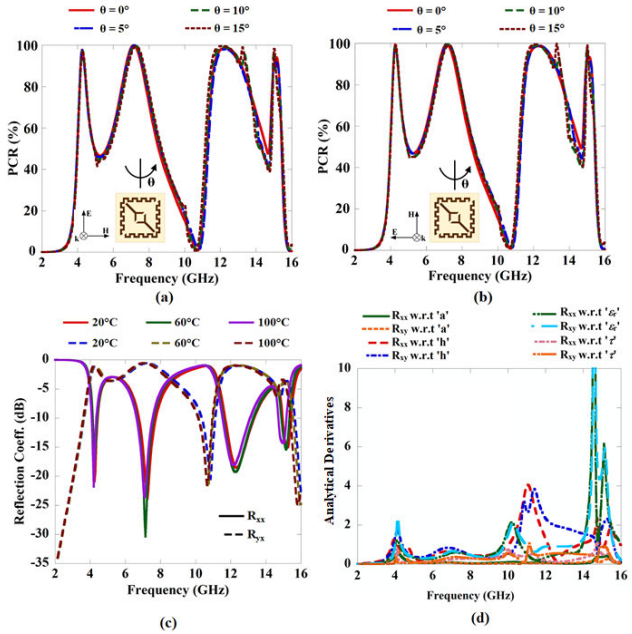

FIGURE 8. The polarization conversion characteristics of proposed metasurface (a) for different incident angle under TE polarization, (b) for different incident angle under TM polarization. (c) Variation of the reflection coefficients under varied temperature conditions (d) Analytical derivatives of the co- and cross-polarization reflection properties with respect to the different material parameters.

observed that the ellipticity is -1 in the frequency bands: 4.75–5.95 GHz and 14.35–14.6 GHz, implying that the incident linear polarized EM wave gets converted to LHCP. Likewise, the ellipticity approximates to $+1$ around the frequency region: 4 GHz and 8.35–8.8 GHz, denoting RHCP is reflected from the surface. Thus, our proposed design succeeds in achieving both linear-to-LHCP and linear-to-RHCP conversion in separate frequency regimes.

To understand the robustness and practicability of the proposed *PCR* structure, the oblique incidence performance of the proposed structure is also performed for both TE and TM polarization and shown in Figure 8(a) and 8(b) respectively. It is observed that the metasurface exhibit a stable performance up to 15^o of oblique incidence. Moreover, the identical response of TE and TM polarized incident wave indicate high degree of stability of our proposed miniaturized structure. To understand the robustness of the metasurface, we simulate the structure with different ambient temperatures and plotted the reflection coefficient in Figure 8(c). It should be mentioned that the permittivity and conductivity of the material vary with the ambient temperature [24]. From Figure 8(c), it is observed that the reflection property of the metasurface does not alter with the variation of temperature. For understanding the sensitivity and tolerance of our proposed design, we performed the analytic derivatives for different material parameters such as permittivity (ε), periodicity (a), copper layer thickness (τ) and thickness of the dielectric layer (h). The analytic derivatives of the co- and cross-polarized reflection coefficient with respect to the aforementioned parameters are

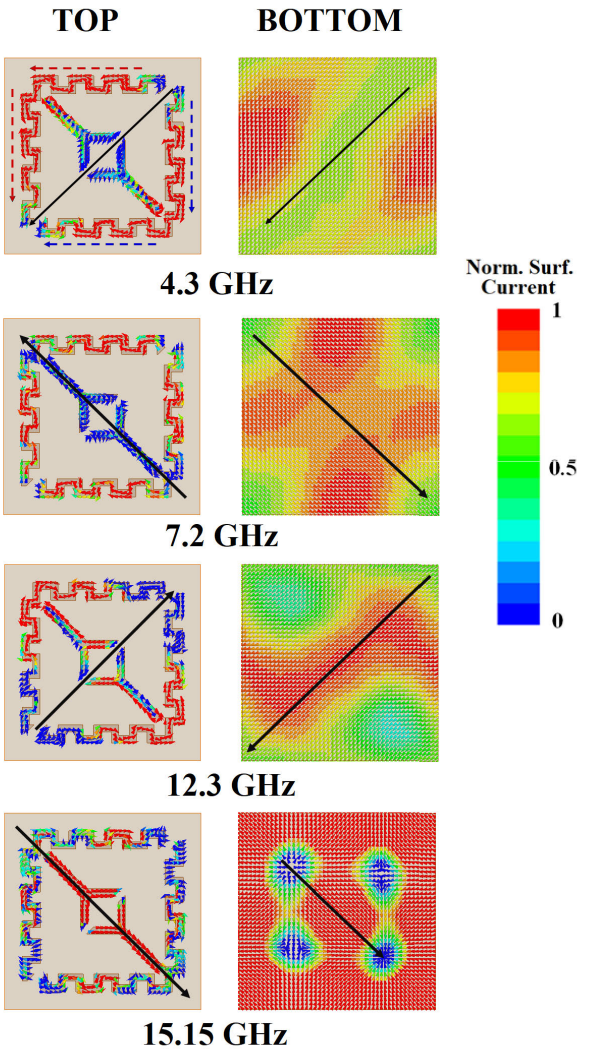

FIGURE 9. Surface current distribution on the top and bottom surface at the LP-LP conversion bands.

shown in Figure 8(d). It is observed that, the permittivity of the dielectric substrate has a significant impact on both co- and cross-polarized reflection coefficients compared to other parameters. Moreover, the sensitivity of these material parameters is more acute in the high-frequency region. This analysis provides a set of guidelines that are required for fabrication.

For getting a clear understanding of the polarization conversion mechanism, here we need to monitor the surface current distribution at each frequency of operation. In Figure 9, we depicted the surface current distribution along the top and bottom surface of the proposed reflective polarization converter at the linear to linear polarization conversion frequency bands. It is seen from the figure that at 4.3 GHz and 7.2 GHz frequency regions, the surface current gets accumulated along the Reso.II structure. On the contrary, Reso.I dominates at 15.15 GHz frequency. However, at 12.3 GHz frequency region, a significant amount of surface

current can be observed to be distributed along both the Reso.I and Reso.II structures. This verifies that the 3rd resonating band is because of the mutual coupling between Reso.I and Reso.II. Such a phenomenon is also witnessed in Figure 5(c).

On another note, it can be spotted at 4.3 GHz frequency that, the surface currents are propagating from the top-right to the top-left, and from the top-left to the bottom-left directions in the upper half of the top layer. A similar pattern is also followed by the surface currents in the lower half of the top surface, flowing from the top-right to the bottom-left but via the bottom-right corner. These are indicated in the figure by the red and blue broken arrow lines at the 4.3 GHz in the upper and lower half respectively. Thus, the resultant surface current in the top surface can be assumed to be propagating diagonally from the top-right corner to the bottom-left corner as represented by the solid black arrow line. Similar type of analysis can also be performed for all the other frequency regions in the top and bottom half of the resultant solid arrow line at the top surface. (To enhance the visibility of the image, we have not included the broken arrows in the following images). In the bottom layer, at 4.3 GHz frequency, the surface currents are also directed from the top-right to the bottom-left direction. Equivalent scenario is also observed at 15.15 GHz frequency, where the surface currents are directed from the top-left to the bottom-right directions in both the top and bottom surfaces. Thus, following the traits of the surface current distributions on the top and bottom plane at these two frequencies, it can be believed that the net currents on the two layers are parallel to each other. This parallel current distribution in the top and bottom layer indicates electric responses behaviour of the structure at the mentioned frequencies [21]. On the contrary, at 7.2 GHz and 12.3 GHz frequencies, we can find that the net currents on the top and bottom layers are directed parallel but opposite to each other, which implies that these currents form a current loop. This current loop induces magnetic field, which gets accumulated within the dielectric layer, leading to the magnetic resonance behaviour of the structure [21].

Figure 10 gives the surface current distributions at the centre frequencies for the linear-to-circular polarization bands, i.e., 4 GHz, 5.3 GHz, 8.5 GHz and 14.5 GHz. The primary feature that can be observed at each of these frequency bands is that, the surface currents in the ground plane align themselves in an orthogonal formation. This is quite different from the case of linear-to-linear polarization, where all the currents in the bottom layer are aligned in a particular diagonal direction. This orthogonal behaviour, which is represented by the solid horizontal and vertical arrow lines in the bottom layer at 4 GHz, 5.3 GHz, 8.5 GHz, and 14.5 GHz in Figure 10, indicates the CP nature of the reflective wave.

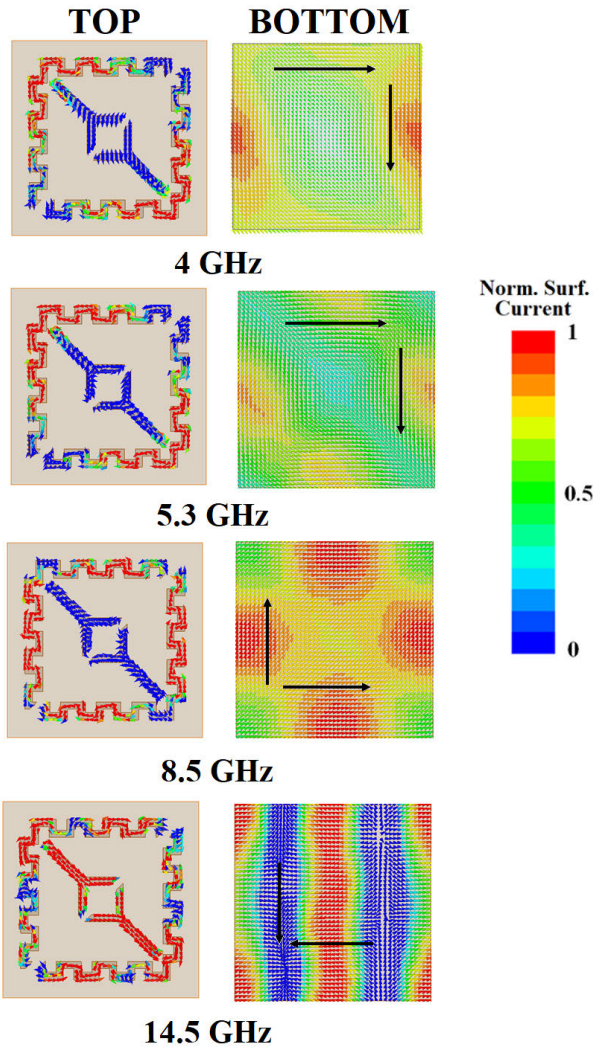

FIGURE 10. Surface current distribution on the top and bottom surface at the LP-CP conversion bands.

III. FABRICATION AND MEASURED RESULTS

For the validation of our proposed design concept, a 10 × 10 array of the unit cell has been fabricated. The photograph of the fabricated prototype is shown in Figure 11(a). The overall size of the metasurface slab is 110 × 110 mm^2. To validate the polarization conversion capability of the proposed metasurface, the co- and cross-polarization reflection coefficients are needed to be measured. In this work, we have used two ridged broadband horn antennas, both connected to the vector network analyzer (VNA). The schematic diagram of the measurement setup is exhibited in Figure 11(b). One horn acts as a transmitting antenna while the other works as a receiving antenna. To measure the co-polarized reflection coefficient, both the transmitting and the receiving horn antennas are in the same orientation. Whereas, for the cross-polarization reflection coefficient measurement, the receiving antenna is placed in vertical state while the transmitting horn antenna is horizontally positioned. The measured R_{xx} and R_{yx} along with the simulated results is shown in Figure 11(c). A close agreement is observed between the simulated and measured results. The slight variations in measured results may be associated with fabrication imperfections, finite size of the reflection polarization converter, and possible errors in the

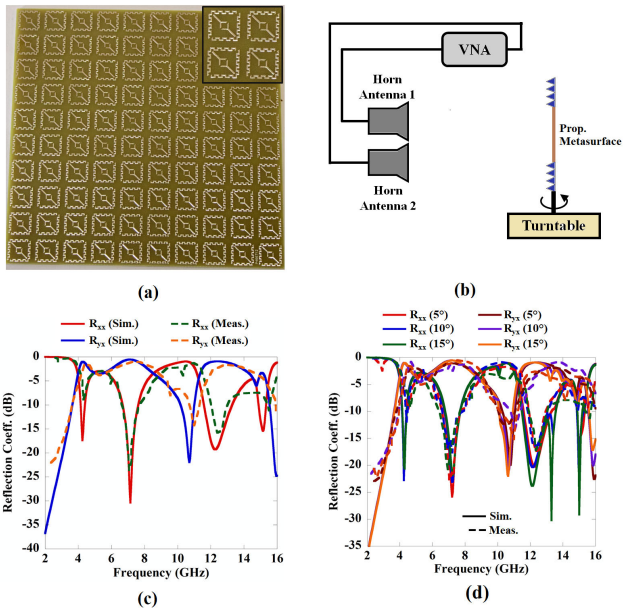

FIGURE 11. **Proposed metasurface based reflective polarization converter (a) Fabricated prototype (b) Schematic set-up for the measurement (c) Simulated and measured co- and cross-polarized reflection coefficients for normal incidence (d) Simulated and measured co- and cross-polarized reflection coefficient for oblique incidence.**

TABLE 2. **Comparison of the proposed reflective polarization converter structure with some earlier reported structures.**

Ref.	Lat. Dim.(λ_o)	Thick. (λ_o)	No. of Bands		Freq. (GHz)	
			LP-LP	LP-CP	LP-LP (PCR $\geq$ 90%)	LP-CP (AR $\leq$ 3dB)
[21]	0.241	0.08	1	1	7.7–14.5	14.95–17.35
[25]	0.252	0.126	2	0	5.66–9.46 16.9–18.9	
[26]	0.446	0.068	2	2	13.29 20.29	14.08–15.71 17.63–19.55
Our Work	0.147	0.042	4	4	4.19–4.40 6.8–7.64, 11.54–13.07, 14.98–15.30	3.95-4.14 4.75–5.95 8.35–8.8 14.35–14.6

measurement set-up. To validate the performance of the metasurface in oblique incidence, we also measured the reflection coefficient for oblique incidences. For this purpose, the metasurface is mounted on a turntable and rotated accordingly. The measured reflection coefficients along with the simulated ones for different oblique incident angles are shown in Figure 11(d), where a stable performance can be observed up to 15^o.

For appreciating the standard of the proposed reflective polarization converter, we have drawn a comparison with the recently reported reflective polarization converters in Table 2. It should be mentioned that to convert the LP to its orthogonal polarization, PCR should be more than 90%. Whereas, for proper LP to CP conversion, AR be considered less than 3 dB. It can be observed from the table that our structure offers better miniaturized design in terms of compactness and thickness. Also, in terms of performance, our structure provides most number of bands having conversions in both linear and circular regimes. In overall, the proposed prototype serves as a better candidate among the others in demanding applications.

IV. CONCLUSION

In summary, we have realized a planar metasurface based multiband reflective polarization converter for both linear-to-linear and linear-to-circular or circular to linear polarization transformation. Due to the anisotropic characteristic of the metasurface, the proposed structure can convert a y/x-polarised incident electromagnetic wave to an x/y-polarised reflected electromagnetic wave in four frequency bands with PCR over 95%. Further, the metasurface can also convert an LP incident wave into a circular configuration in another four frequency bands with less than 3 dB axial ratio. The proposed octa-band reflective polarization converter is made up of meandered square split ring resonator and diagonal strip structure, which gets multiple resonances, enabling the metasurface to achieve polarization transformation in multiple bands. Parametric studies and analytic derivatives with respect to the different parameters are given in details to serve as a guide for the design. Moreover, a step-by-step design procedure is explained for providing an insight in the design procedure. A study of the induced surface current distributions along with a rigorous theoretical analysis is presented to explain the operating principle of the polarization conversions. This reflective polarization converter structure covers most of the C,X and K_u bands. All the simulation results are verified through experimental measurements.

REFERENCES

[1] R. Dutta, S. C. Bakshi, and D. Mitra, "An ultrathin compact polarization-insensitive hepta-band absorber," in *IEEE MTT-S Int. Microw. Symp. Dig.*, Nov. 2018, pp. 1–4.

[2] G. Samanta, J. Ghosh, T. Shaw, and D. Mitra, "Design of a polarization insensitive wideband absorber using graphene based metasurface," *Prog. Electromagn. Res. Lett.*, vol. 86, pp. 27–33, 2019.

[3] D. Schurig, J. J. Mock, B. J. Justice, S. A. Cummer, J. B. Pendry, A. F. Starr, and D. R. Smith, "Metamaterial electromagnetic cloak at microwave frequencies," *Science*, vol. 314, no. 5801, pp. 977–980, Oct. 2006.

[4] J. Ghosh and D. Mitra, "Restoration of antenna performance in the vicinity of metallic cylinder in implantable scenario," *IET Microw., Antennas Propag.*, vol. 14, no. 12, pp. 1440–1445, Oct. 2020.

[5] J. Pendry, "Negative refraction makes a perfect lens," *Phys. Rev. Lett.*, vol. 85, no. 18, p. 3966, 2000.

[6] S. Maslovski and S. Tretyakov, "Phase conjugation and perfect lensing," *J. Appl. Phys.*, vol. 94, no. 7, pp. 4241–4243, Sep. 2003.

[7] J. Hao, Y. Yuan, L. Ran, T. Jiang, J. A. Kong, C. T. Chan, and L. Zhou, "Manipulating electromagnetic wave polarizations by anisotropic metamaterials," *Phys. Rev. Lett.*, vol. 99, Aug. 2007, Art. no. 063908.

[8] R. Dutta, D. Mitra, and J. Ghosh, "Dual-band multifunctional metasurface for absorption and polarization conversion," *Int. J. RF Microw. Comput.-Aided Eng.*, vol. 30, no. 7, Jul. 2020, Art. no. e22200.

[9] J. Ren, W. Jiang, K. Zhang, and S. Gong, "A high-gain circularly polarized Fabry–Perot antenna with wideband low-RCS property," *IEEE Antennas Wireless Propag. Lett.*, vol. 17, no. 5, pp. 853–856, May 2018.

[10] L. Zhang, C. Liu, C. Ni, M. Kong, and X. Wu, "Low-RCS, circular polarization, and high-gain broadband antenna based on mirror polarization conversion metasurfaces," *Int. J. Antennas Propag.*, vol. 2019, pp. 1–8, Aug. 2019.

[11] C. F. Fu, L. F. Han, C. Liu, Z. J. Sun, and X. L. Lu, "Dual-band polarization conversion metasurface for RCS reduction," *IEEE Trans. Antenn. Propag.*, vol. 69, no. 5, pp. 3044–3049, May 2021.
[12] Y. Jia, Y. Liu, Y. J. Guo, K. Li, and S.-X. Gong, "Broadband polarization rotation reflective surfaces and their applications to RCS reduction," *IEEE Trans. Antennas Propag.*, vol. 64, no. 1, pp. 179–188, Jan. 2016.
[13] Y. Zhao and A. Alù, "Manipulating light polarization with ultrathin plasmonic metasurfaces," *Phys. Rev. B, Condens. Matter*, vol. 84, Nov. 2011, Art. no. 205428.
[14] H. Sun, C. Gu, X. Chen, Z. Li, L. Liu, and F. Martín, "Ultra-wideband and broad-angle linear polarization conversion metasurface," *J. Appl. Phys.*, vol. 121, no. 17, May 2017, Art. no. 174902.
[15] Z. L. Mei, X. M. Ma, C. Lu, and Y. D. Zhao, "High-efficiency and wide-bandwidth linear polarization converter based on double U-shaped metasurface," *AIP Adv.*, vol. 7, no. 12, Dec. 2017, Art. no. 125323.
[16] L. Wu, Z. Yang, Y. Cheng, R. Gong, M. Zhao, Y. Zheng, J. Duan, and X. Yuan, "Circular polarization converters based on bi-layered asymmetrical split ring metamaterials," *Appl. Phys. A, Solids Surf.*, vol. 116, no. 2, pp. 643–648, Feb. 2014.
[17] Y. Li, J. Zhang, S. Qu, J. Wang, and L. Zheng, "Achieving wide-band linear-to-circular polarization conversion using ultra-thin bi-layered metasurfaces," *J. Appl. Phys.*, vol. 117, no. 4, 2015, Art. no. 044501.
[18] Y. Huang, L. Yang, J. Li, Y. Wang, and G. Wen, "Polarization conversion of metasurface for the application of wide band low-profile circular polarization slot antenna," *Appl. Phys. Lett.*, vol. 109, no. 5, Aug. 2016, Art. no. 054101.
[19] O. Fernández, A. Gómez, J. Basterrechea, and A. Vegas, "Reciprocal circular polarization handedness conversion using chiral metamaterials," *IEEE Antennas Wireless Propag. Lett.*, vol. 16, pp. 2307–2310, 2017.
[20] B. Lin, J. Guo, L. Lv, J. Wu, Y. Ma, B. Liu, and Z. Wang, "Ultra-wideband and high-efficiency reflective polarization converter for both linear and circular polarized waves," *Appl. Phys. A, Solids Surf.*, vol. 125, no. 2, p. 76, 2019.
[21] Q. Zheng, C. Guo, G. A. E. Vandenbosch, P. Yuan, and J. Ding, "Dual-broadband highly efficient reflective multi-polarisation converter based on multi-order plasmon resonant metasurface," *IET Microw., Antennas Propag.*, vol. 14, no. 9, pp. 967–972, Jul. 2020.
[22] M. I. Khan, Z. Khalid, S. A. K. Tanoli, F. A. Tahir, and B. Hu, "Multiband linear and circular polarization converting anisotropic metasurface for wide incidence angles," *J. Phys. D, Appl. Phys.*, vol. 53, no. 9, Feb. 2020, Art. no. 095005.
[23] C. Mao, Y. Yang, X. He, J. Zheng, and C. Zhou, "Broadband reflective multi-polarization converter based on single-layer double-L-shaped metasurface," *Appl. Phys. A, Solids Surf.*, vol. 123, p. 767, Dec. 2017.
[24] V. V. Varadan and L. Ji, "Temperature dependence of resonances in metamaterials," *IEEE Trans. Microw. Theory Techn.*, vol. 58, no. 10, pp. 2673–2681, Oct. 2010.
[25] M. Yan, J. Wang, Y. Pang, C. Xu, H. Chen, L. Zheng, J. Zhang, and S. Qu, "An FSS-backed dual-band reflective polarization conversion metasurface," *IEEE Access*, vol. 7, pp. 104435–104442, 2019.
[26] Y. Yu, F. Xiao, C. He, R. Jin, and W. Zhu, "Double-arrow metasurface for dual-band and dual-mode polarization conversion," *Opt. Exp.*, vol. 28, no. 8, pp. 11797–11805, 2020.

RAHUL DUTTA was born in West Bengal, India, in 1993. He received the B.Tech. degree in electronics and communication engineering from the West Bengal University of Technology, Kolkata, India, in 2016, and the M.Tech. degree in electronics and telecommunication engineering from the Indian Institute of Engineering Science and Technology (IIEST), Shibpur, India, in 2019. He is currently pursuing the Ph.D. degree in electronic engineering with the School of Electronic Engineering and Computer Science, Queen Mary University of London, U.K.

His research interests include metamaterials and metasurfaces, microwave absorbers, polarization converters, reconfigurable structures, frequency selective surfaces, and antennas.

JEET GHOSH received the B.Tech. degree in electronics and communication engineering from the West Bengal University of Technology, Kolkata, India, in 2011, the M.Tech. degree in electronics and communication engineering (specialization in microwave engineering) from The University of Burdwan, Burdwan, India, in 2013, and the Ph.D. degree in electronics and telecommunication engineering from the Indian Institute of Engineering Science and Technology, Shibpur, India, in 2020.

He has published numerous papers in the areas of MIMO antennas, mutual coupling in array antennas, circular polarized antennas, metamaterial, and so on. His current research interests include MIMO antennas, antenna array, frequency-selective surfaces (FSS), biomedical implantable antennas, and wireless power transfer technique. He was a recipient of the SRF Award from the Council of Scientific and Industrial Research (CSIR), India. He also serves as a Reviewer for different journal, like *International Journal of RF and Microwave Computer-Aided Engineering*, *IET Microwaves, Antennas and Wave Propagation*, *Progress in Electromagnetics Research*, and so on.

ZHENGBAO YANG (Member, IEEE) received the bachelor's degree from the Harbin Institute of Technology, in 2012, and the Ph.D. degree from the University of Toronto, in 2016.

He joined the City University of Hong Kong as an Assistant Professor, in 2017. His research interests include vibration and mechatronics with a special focus on the development of smart structures and dynamical systems for energy harvesters, wireless power transfer, and sensors and actuators. This interdisciplinary research area requires combining the knowledge and skills in mechanical design, electrical circuit, smart materials, and dynamic analysis.

XINGQI ZHANG (Member, IEEE) received the B.Sc. degree from the Harbin Institute of Technology, China, in 2012, and the M.A.Sc. and Ph.D. degrees from the University of Toronto, Canada, in 2014 and 2018, respectively.

He is currently an Assistant Professor with the School of Electrical and Electronic Engineering, University College Dublin, Ireland. He is also affiliated with the Department of Electrical and Computer Engineering, University of Toronto, as a Visiting Professor. His research interests include the fundamental and applied aspects of computational electromagnetics and wireless communications. A particular focus is on wireless channel modeling and optimization in indoor, urban, and terrestrial environments, multiphysics/multiscale modeling for electromagnetic, micro-/nano-electronic, and biomedical problems, stochastic uncertainty quantification and machine learning, EMC/EMI analysis, reconfigurable intelligent surface, and antenna/RF design and measurement.

Dr. Zhang was a recipient of the RIA Charlemont Award from the Royal Irish Academy, the Young Scientist Award from the International Union of Radio Science (URSI), and several best paper awards at international symposia. He has served as a TPC member and the session chair for several high-profile conferences. He has served as an Associate Editor for the IEEE JOURNAL ON MULTISCALE AND MULTIPHYSICS COMPUTATIONAL TECHNIQUES.